IEEE Access
Multidisciplinary ⋮ Rapid Review ⋮ Open Access Journal

Received 3 May 2024, accepted 5 July 2024, date of publication 9 July 2024, date of current version 17 July 2024.

Digital Object Identifier 10.1109/ACCESS.2024.3425462

RESEARCH ARTICLE

Adaptive Fault-Tolerant Finite-Time Flight-Path Angle Control for Aircraft Systems With Unknown Deadzone and Actuator Faults

YOUFANG YU AND LIYANG WANG
Applied Engineering College, Zhejiang Business College, Hangzhou 310053, China

Corresponding author: Youfang Yu (youfang_yu@163.com)

This work was supported by Zhejiang Provincial Natural Science Foundation of China under Grant LY22F030011 and Grant LZ22F030008.

ABSTRACT This study focuses on fault-tolerant finite-time flight-path angle control for an aircraft in the presence of external disturbances, unknown deadzone and actuator fault. To begin with, the longitudinal model of aircraft is introduced for the subsequent controller design. Then, a new smooth deadzone inverse model is presented to compensate for the deadzone nonlinearity in aircraft system. A robust adaptive fault-tolerant finite-time control law is derived by using backstepping adaptive control approach, where a finite-time stability criterion is adopted for developing practical finite-time control. In order to reduce the difficulty of control system design, two finite-time differentiators are used to estimate the derivatives of virtual control signals. The coupling errors of the deadzone and faults are properly dealt with by estimating the unknown bounds. Finally, comparative numerical simulation results are provided to demonstrate the efficiency of the proposed fault-tolerant finite-time flight-path angle control scheme.

INDEX TERMS Adaptive control, flight path angle, finite-time tracking, deadzone inverse compensation, fault-tolerant control.

I. INTRODUCTION

Along with the rapid development of aviation technology and aircraft manufacturing industry, aircrafts are more and more widely used in martial and civil fields. In recent years, the research on aircraft control technology has been one of the hot topics. Due to fuel consumption and body deformation during aircraft cruising, it is quite difficult to get a precise model of aircraft system. In addition, there still exist high nonlinearities and strong coupling in aircraft dynamics. These disadvantages make the control issue of aircraft challenging and nontrivial. Therefore, the precise control of aircraft is still an open topic to be tackled.

In order to achieve better performance in aircraft trajectory angle control, great efforts have been made to improve control technique and exploit new methods. In [1], neuro-adaptive backstepping method is developed for the control of flight-path angle. In [2], two nonlinear control techniques are used in the design of flight-path tracking control laws for a transport aircraft. In [3], an adaptive dynamic surface controller was proposed for flight-path angle control. In [4], an adaptive backstepping terminal sliding mode control method for the control of flight-path angle was developed. In [5], a neural-network based adaptive dynamic surface control solution was presented for the flight-path angle control of an aircraft with parameter uncertainties, multi-disturbances and nonlinearities. These studies have strongly promoted the development of aircraft flight-path angle control techniques.

In most of the above results, the tracking errors can converge to a small neighborhood of origin as time goes to infinity. To make the tracking error converge to the origin or its small neighborhood within a finite time, some scholars have studied advanced control algorithms during controller design for nonlinear systems [6], [7], [8]. In the context of aircraft control, there exist a few literature results

The associate editor coordinating the review of this manuscript and approving it for publication was Qi Zhou.

concerned with finite-time control design for improving convergence speed [9], [10], [11], [12], [13], [14], [15], [16]. Among these algorithms, the adopted control strategies mainly focus on terminal sliding mode control, predefined time control, etc. As far as flight-path angle finite-time convergence is concerned, the research on flight-path angle finite-time convergence is still very few at present, and the obtained results are mainly involved with backstepping terminal sliding control [4], whose design is comparatively complicated. In [6], Sun et al proposed a new finite time stability criterion to easily design finite-time control law for a class of nonstrict feedback systems. To the best of our knowledge, hitherto, few literature results involved with flight-path angle control design according to this finite-time stability criterion have been reported. How to develop an effective control scheme according to this finite-time stability criterion is still unclear.

In controller design and control system analysis, to achieve good performance, the effect of non-smooth nonlinearities (saturation, deadzone, backlash and hysteresis) in actuators should be taken into consideration [17], [18]. As the most common nonlinearities, deadzones widely exist in the actuators of many mechanical device and electrical equipments, which damages the performance of control systems more or less, and even leads to system instability in severe cases. Therefore, it is of urgent need to take appropriate compensation to offset the effects caused by deadzones. So far, there have roughly been three mainstream strategies for deadzone compensation. The first one is robust compensation method, in which the deadzone is modeled as a combination of a linear term and a disturbance-like term, and the deadzone slopes in positive and negative are assumed to be same [19]. Afterwards, Ibrir et al. proposed an adaptive robust control algorithm suitable for asymmetric deadzone situations [20]. Another alternative approach is to apply neural networks or fuzzy systems to approximate deadzones [21], [22]. The third strategy is the adaptive compensation method based on deadzone inverse model. The study in this aspect was initiated in [23], where a discontinuous deadzone inverse model is constructed to compensate for the actuator deadzone. Chattering phenomenon may easily occur if non-smooth inverse is used for controller design. For overcoming this disadvantage, a smooth adaptive deadzone inverse model has been built to offset the effect of unknown deadzone [24]. Inspired by this, scholars have proposed some other inverse model construction schemes [25], [26]. As for aircraft control, robust compensation strategies are adopted for dealing with deadzones in most related algorithms [27]- [30], However, few research results on inverse model compensation for aircraft deadzones have been reported.

Reliability plays an important role in the design and operation of modern industrial engineering systems. Given that a local fault may unexpectedly affect the entire system, appropriate actions should be taken during the controller design process to avoid the performance degradation of closed-loop system. For this reason, fault-tolerant control has become an increasingly important research topic for its advantage of maintaining expected system performance even if potential faults occur. Some fault-tolerant control methods have been proposed for aircraft systems in the past few years. In [31], Fekih proposed a fault-tolerant control approach which can simultaneously compensate for actuator faults, model mismatch and parameter variations in aircraft systems. In [32], an aircraft fault-tolerant trajectory controller is developed, with the incremental nonlinear dynamic inversion approach used to deal with the uncertainties. In [33], based on sliding mode and adaptive techniques, a fault-tolerant flight control scheme against actuator failures is proposed by incorporating both the actuator amplitude and rate bounds. Overall, in the context of aircraft flight-path angle control, the research achievements on fault-tolerant control have been still few.

In many practical engineering systems, actuators are simultaneously affected by actuator faults and deadzone nonlinearities [34], [35]. To the best of our knowledge, despite rapid progresses having been made in aircraft control, there is a paucity of research on offsetting the hybrid effects of unknown deadzone nonlinearities and actuator faults in aircraft control system designs. How to address the issue of flight-path angle control for an aircraft system subject to both unknown deadzone and actuator fault, while meeting the requirement of finite-time convergence, is a challenging research topic.

Motivated by above discussion, this paper investigates the flight-path angle control algorithms for aircraft systems with deadzone nonlinearity and actuator faults. The main contributions of this study are as follows.

1) A practical finite-time control algorithm is developed to solve the flight-path angle tracking problem for aircrafts, where no sliding mode surface is constructed and two finite-time differentiators are used to estimate the derivatives of virtual control signals, simplying the control system design.
2) In the existing results on flight-path angle control [1], [2], [3], [4], [5], neither unknown deadzone nonlinearity nor actuator faults were considered. In this work, both unknown deadzone nonlinearity and actuator faults are considered during controller design.
3) A new smooth deadzone inverse model is constructed to implement the compensation for unknown deadzone nonlinearity in the aircraft system.

The remainder of this article is organized as follows. In Section II, the longitudinal model of aircraft is established, and the problem of flight path-angle control is formulated, with standard assumptions, definition and lemmas. Then, a smooth deadzone inverse, the detailed design procedure of finite-time controller, and the stability analysis are presented in Section III. Thereafter, in Section IV, an illustrative example is presented to demonstrate the effectiveness of the proposed control method. Finally, concluding remarks are given in Section V.

II. PROBLEM FORMULATION

In longitudinal aircraft dynamics, the flight path stands for the route of an aircraft moving forward relative to the ground. The direction of the flight path is called flight-path angle, whose mathematical definition is as follows [1]:

$$\gamma = \sin^{-1}\left(\frac{\dot{h}}{V_T}\right), \tag{1}$$

in which $\dot{h}$ is the rate of change in altitude, and V_T is the aircraft's airspeed. The time derivative of γ is determined by

$$\begin{aligned}\dot{\gamma} = \frac{1}{mV_T}&(L\cos\mu - D\sin\beta\sin\mu - Y\sin\mu\cos\beta \\ &+ F_T(\sin\alpha\cos\mu + \cos\alpha\sin\beta\sin\mu) - mg\cos\gamma)\end{aligned} \tag{2}$$

where F_T is thrust; L, D, and Y are lift force, drag force, and lateral force, respectively; α, β and μ are angle of attack, sideslip angle, and stability-axis roll angle, respectively; m and g are the mass and gravity coefficient of the aircraft, respectively.

In this work, the longitudinal motion of the aircraft is considered, i.e., the aircraft motion is restricted to the pitch plane. In this situation, $Y = \beta = \mu = 0$,

$$\gamma = \theta_p - \alpha, \tag{3}$$

and

$$\dot{\gamma} = \dot{\theta}_p - \dot{\alpha} \tag{4}$$

hold, where θ_p is angle of pitch. The dynamics of α and θ_p are defined by

$$\begin{cases}\dot{\alpha} = \dfrac{1}{mV_T}(-F_T\sin\alpha - L + mg\cos\gamma) + q, \\ \dot{\theta}_p = q,\end{cases} \tag{5}$$

where q is pitch angular velocity. In (5), the thrust term $F_T\sin\alpha$ is much smaller than the lift term L, so $F_T\sin\alpha$ can be neglected in system analysis and controller design. L is regarded as the sum of two following terms:

$$L = L_o + L_\alpha\alpha, \tag{6}$$

where L_α is the slope of the lift curve, and L_o is the contributions of all other factors to lift [1]. Up to this point, a simplified aircraft longitudinal model is given as follows:

$$\begin{cases}\dot{\gamma} = \bar{L}_\alpha\alpha - \dfrac{g}{V}\cos\gamma + \bar{L}_o, \\ \dot{\alpha} = q + \dfrac{g}{V_T}\cos\gamma - \bar{L}_\alpha\alpha - \bar{L}_o, \\ \dot{\theta}_p = q, \\ \dot{q} = M_o + M_\delta\delta,\end{cases} \tag{7}$$

where δ is rudder deflection, $\bar{L}_o = \frac{L_o}{mV_T}$, $\bar{L}_\alpha = \frac{L_\alpha}{mV_T}$, M_δ is pitch control moment coefficient, and M_o is another moment which usually can be estimated by $M_o = M_\alpha\alpha + M_q q$. V_T, γ, α, θ_p and δ are depicted in Figure 1. In this work, M_α, M_δ, M_q, L_α, L_o, m, g, δ and V_T are considered constant and unknown.

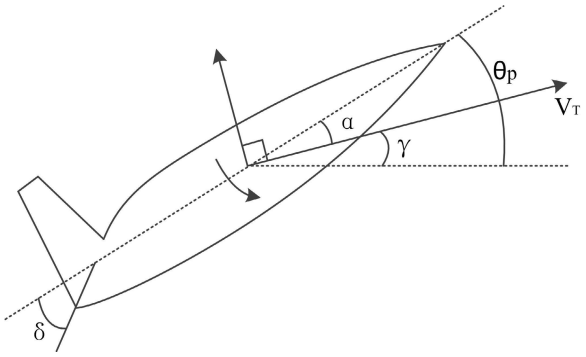

FIGURE 1. Schematic diagram of longitudinal model of aircraft.

Let $x_1 = \gamma, x_2 = \theta_p$ and $x_3 = q$. Given that there exist external disturbances, the aircraft longitudinal model may be rewritten as

$$\begin{cases}\dot{x}_1 = a_1(x_2 - x_1) + a_2 - a_3\cos x_1 + \Delta_1(t), \\ \dot{x}_2 = x_3, \\ \dot{x}_3 = b_1\delta + b_2(x_2 - x_1) + b_3x_3 + \Delta_2(t),\end{cases} \tag{8}$$

where $a_1 = \bar{L}_\alpha > 0$, $a_2 = \bar{L}_o$, $a_3 = \frac{g}{V_T}$, $b_1 = M_\delta > 0$, $b_2 = M_\alpha$, $b_3 = M_q$, and $\Delta_1(t)$ and $\Delta_2(t)$ are unknown but bounded disturbances.

By taking the effect of unknown dead-zone nonlinearity and actuator faults into account, the actuator expression is described as

$$\delta = \rho_f u(v) + \phi_f \tag{9}$$

where $\rho_f \in (0, 1]$ denotes multiplicative actuator fault and ϕ_f denotes the additive actuator fault, and $u(v)$ is the output of deadzone nonlinearity as

$$u(v) = \begin{cases} m_r(v - b_r), & \text{if } v \geq b_r, \\ 0, & \text{if } b_r < v < b_l, \\ m_l(v - b_l), & \text{if } v \leq b_l, \end{cases} \tag{10}$$

in which $b_r \geq 0$, $b_l \leq 0$ and $m_r > 0$, $m_l < 0$ are unknown constants, v is the input and $u(v)$ the output. A graphical representation of the deadzone is shown in Figure 2.

The control target of this paper is to present a robust adaptive fault-tolerant finite-time flight-path angle control scheme for an aircraft with unknown deadzone and actuator faults such that x_1 can track the reference trajectory $x_{1,d}$.

Before the controller design, two assumptions, a definition and some lemmas used in this paper are given as follows:

Assumption 1: The lower bounds of unknown deadzone slopes m_r and m_l are known, i.e., there exist two known positive constants m_{r0} and m_{l0}, satisfying $m_r \geq m_{r0}$ and $m_l \geq m_{l0}$.

Definition 1 ([6]): Let $\boldsymbol{\kappa} = \mathbf{0}$ be the equilibrium point of a nonlinear system $\dot{\boldsymbol{\kappa}} = \boldsymbol{f}(\boldsymbol{\kappa})$. If there are a positive constant ε_c and a bounded settling time $T(\varepsilon_c, \boldsymbol{\kappa}_0)$ such that under the arbitrary initial condition $\boldsymbol{\kappa}(t_0) = \boldsymbol{\kappa}_0$, $\|\boldsymbol{\kappa}(t)\| < \varepsilon_c$ holds while $t > t_0 + T(\varepsilon_c, \boldsymbol{\kappa}_0)$, then this system is called a semiglobal practical finite-time stable (SGPFS) system.

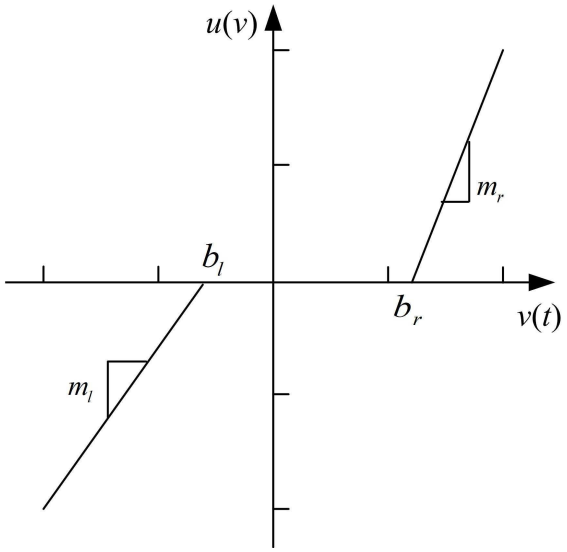

FIGURE 2. Ideal deadzone model.

Lemma 1 [6]: Consider a nonlinear system $\dot{\boldsymbol{\kappa}} = \boldsymbol{f}(\boldsymbol{\kappa})$. Suppose that there exist a smooth positive definite function $\boldsymbol{f}(\boldsymbol{\kappa})$ and some scalars $\tau_1 > 0, 0 < \tau_2 < 1$ and $0 < \tau_3$ such that

$$V(\boldsymbol{\kappa}) < -\tau_1 V^{\tau_2}(\boldsymbol{\kappa}) + \tau_3, t \geq 0, \tag{11}$$

then $\dot{\boldsymbol{\kappa}} = \boldsymbol{f}(\boldsymbol{\kappa})$ is a SGPFS system. For $t \geq T_r, \boldsymbol{\kappa} \in \Omega_\kappa$ holds, where $T_r = \frac{1}{(1-\tau_2)\tau_1 c_0}[V^{1-\tau_2}(\boldsymbol{\kappa}(0)) - \frac{\tau_3}{\tau_1(1-c_0)}^{\frac{1-\tau_2}{\tau_2}}]$, $\Omega_\kappa = \{\boldsymbol{\kappa} | V^{\tau_2}(\boldsymbol{\kappa}) \leq \frac{\tau_3}{\tau_1(1-c_0)}\}, 0 < c_0 < 1$.

Lemma 2 [36]: For $h \in \mathbb{R}$ and $p > 0$,

$$0 \leq |h| - \frac{h^2}{\sqrt{h^2 + p^2}} < p\Upsilon \tag{12}$$

holds, where $\Upsilon = \sqrt{0.5(5\sqrt{5} - 11)} \approx 0.3$.

Lemma 3 [38]: Consider the following finite-time second-order differentiator:

$$\begin{cases} \dot{\zeta}_1 = \zeta_2 \\ \varepsilon^2 \dot{\zeta}_2 = -\text{sat}_{\epsilon_b}\big(\text{sign}(\phi_\alpha(\zeta_1, \kappa(t), \varepsilon\zeta_2))|\phi_\alpha(\zeta_1, \kappa(t), \varepsilon\zeta_2)|^{\iota_1}\big) \\ -\text{sat}_{\epsilon_b}\big(\text{sign}(\zeta_2)|\varepsilon\zeta_2)|^{\mu}\big), \end{cases}$$

where $\varepsilon > 0, 0 < \mu < 1, \iota_1 = \frac{\mu}{2-\mu}$,

$$\phi_\alpha(\zeta_1, \kappa(t), \varepsilon\zeta_2) = \zeta_1 - \kappa(t) + \frac{\text{sign}(\zeta_2)|\varepsilon\zeta_2)|^{2-\mu}}{2-\mu}, \tag{13}$$

$$\text{sat}_*(\bullet) \triangleq \begin{cases} \bullet, & \text{if } |\bullet| < *, \\ *\text{sign}(\bullet), & \text{if } |\bullet| \geq *. \end{cases} \tag{14}$$

For a continuous and piecewise two-order derivable signal $v(t)$, there exists $\iota_2 > 0$ satisfying $\iota_1\iota_2 > 2$, such that

$$\zeta_i - \kappa^{(i-1)}(t) = O(\varepsilon^{\iota_1\iota_2 - i + 1}) \tag{15}$$

can be determined in a finite time.

Lemma 4 [39]: For any real variables ς and ψ, we have

$$|\varsigma|^{c_1}|\psi|^{c_2} \leq \frac{c_1}{c_1 + c_2}c_3|\varsigma|^{c_1+c_2} + \frac{c_1}{c_1 + c_2}c_3^{-\frac{c_1}{c_2}}|\psi|^{c_1+c_2}, \tag{16}$$

where c_1, c_2, and c_3 are positive constants.

Lemma 5 For a real number $0 < \vartheta \leq 1$ and $w_i \in \mathbb{R}$, $i = 1, 2, \cdots, m$, the following inequality holds:

$$(\sum_{i=1}^{m} |w_i|)^{\vartheta} \leq \sum_{i=1}^{m} |w_i|^{\vartheta} \leq m^{(1-\vartheta)}(\sum_{i=1}^{m} |w_i|)^{\vartheta}. \tag{17}$$

In this paper, the arguments of functions are possibly omitted in the cases that no confusion arises.

Remark 1 [37]: In controller design, a smaller upper bound can be achieved by using (12) instead of the following inequality:

$$0 \leq |h| - \frac{h^2}{\sqrt{h^2 + p^2}} < p. \tag{18}$$

III. MAIN RESULT

A. SMOOTH INVERSE MODEL FOR ACTUATOR DEADZONE

By defining

$$\sigma_r(t) = \begin{cases} 1, & u(v) > 0, \\ 0, & \text{otherwise} \end{cases} \tag{19}$$

and

$$\sigma_l(t) = \begin{cases} 1, & u(v) < 0, \\ 0, & \text{otherwise}, \end{cases} \tag{20}$$

we can rewrite (10) as

$$v = \frac{u(v) + m_r b_r}{m_r}\sigma_r(t) + \frac{u(v) + m_l b_l}{m_l}\sigma_l(t) \tag{21}$$

which can be parameterized as

$$u(v) = -\boldsymbol{\varpi}^T \boldsymbol{\omega}, \tag{22}$$

with $\boldsymbol{\varpi} = [m_r, m_r b_r, m_l, m_l b_l]^T, \boldsymbol{\omega} = [-\sigma_r(t)v, \sigma_r(t), -\sigma_l(t)v, \sigma_l(t)]^T$. Note that m_r, b_r, m_l, b_l are unknown while $\sigma_r(t)$ and $\sigma_r(t)$ are unavailable. To offset the effect of deadzone, a new smooth deadzone inverse (the solid line in Figure 3) is proposed as follows:

$$v = \frac{u_d + \widehat{m_r b_r}}{\widehat{m_r}}\phi_r(u_d) + \frac{u_d + \widehat{m_l b_l}}{\widehat{m_l}}\phi_l(u_d), \tag{23}$$

where u_d is the input of inverse model, and $\phi_r(\cdot)$ and $\phi_l(\cdot)$ are defined as follows: For $z \in \mathbb{R}$,

$$\phi_r(z) = \frac{1}{2} + \frac{1}{2}(\frac{z}{|z| + \ell}),$$
$$\phi_l(z) = \frac{1}{2} - \frac{1}{2}(\frac{z}{|z| + \ell}),$$

in which

$$\ell = \begin{cases} 0, & \text{if } |z| \geq \sqrt{\wp}, \\ \sqrt{\wp - z^2}, & \text{if } |z| < \sqrt{\wp}, \end{cases} \tag{24}$$

with $\wp > 0$ being a design parameter.

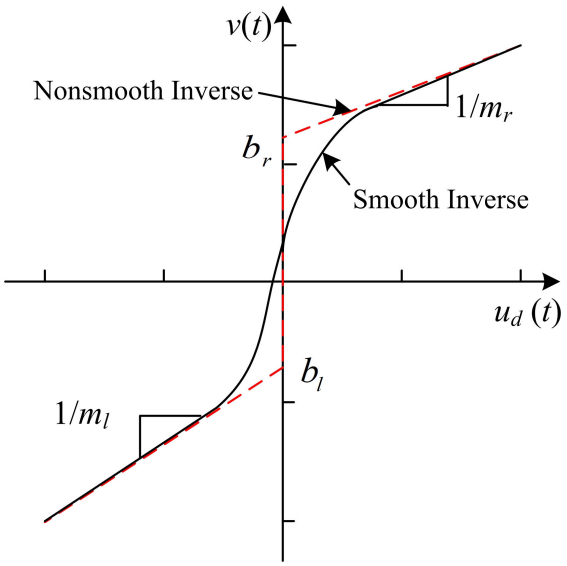

FIGURE 3. Deadzone inverse.

From (23), we can get

$$u_d = -\hat{\boldsymbol{\varpi}}^T \hat{\boldsymbol{\omega}}, \tag{25}$$

where $\hat{\boldsymbol{\varpi}} = [\widehat{m_r}, \widehat{m_r b_r}, \widehat{m_l}, \widehat{m_l b_l}]^T, \hat{\boldsymbol{\omega}} = [-\phi_r(v)v, \phi_r(v), -\phi_l(v)v, \phi_l(v)]^T$. On the basis of (22) and (25), we obtain

$$\begin{aligned} u(v) - u_d &= -\boldsymbol{\varpi}^T \boldsymbol{\omega} + \hat{\boldsymbol{\varpi}}^T \hat{\boldsymbol{\omega}} \\ &= (\hat{\boldsymbol{\varpi}} - \boldsymbol{\varpi})^T \hat{\boldsymbol{\omega}} + \boldsymbol{\varpi}^T \hat{\boldsymbol{\omega}} - \boldsymbol{\varpi}^T \boldsymbol{\omega} \end{aligned} \tag{26}$$

in which $d_u = \boldsymbol{\varpi}^T \hat{\boldsymbol{\omega}} - \boldsymbol{\varpi}^T \boldsymbol{\omega}$. There exists an unknown positive number $\bar{d}_u$, satisfying $|d_u| \le \bar{d}_u$ for $t \ge 0$ [24].

Thus, by combining (9) with (26), the actual fault model is expressed as

$$\delta = \rho_f(u_d + (\hat{\boldsymbol{\varpi}} - \boldsymbol{\varpi})^T \hat{\boldsymbol{\omega}} + d_u) + \phi_f. \tag{27}$$

B. BACKSTEPPING CONTROL DESIGN

Let $z_1 = x - x_{1,d}$, $z_2 = x_2 - \alpha_1$, $z_3 = x_3 - \alpha_2$. For $i = 1, 2$, α_i are virtual control laws to be designed.

Define

$$V_1 = \frac{1}{2a_1} z_1^2. \tag{28}$$

Taking the derivative of V_1 with respect to time yields

$$\begin{aligned} \dot{V}_1 &= z_1(x_2 - x_1 + \frac{a_2}{a_1} - \frac{a_3}{a_1}\cos x_1 + \frac{\Delta_1(t)}{a_1} - \frac{\dot{x}_{1,d}}{a_1}) \\ &= z_1(z_2 + \alpha_1 - x_1 + \boldsymbol{\eta}_1^T \boldsymbol{\varphi}_1 + \frac{\Delta_1(t)}{a_1}), \end{aligned} \tag{29}$$

where $\boldsymbol{\eta}_1 = [\frac{a_2}{a_1}, -\frac{a_3}{a_1}, -\frac{1}{a_1}]^T, \boldsymbol{\varphi}_1 = [1, \cos x_1, \dot{x}_{1,d}]^T$. On the basis of (29), we design the virtual control law as

$$\alpha_1 = x_1 - \hat{\boldsymbol{\eta}}_1^T \boldsymbol{\varphi}_1 - \frac{\varrho_1}{2^F} z_1^{2F-1} - \frac{\hat{\rho}_1^2 z_1}{\sqrt{z_1^2 \hat{\rho}_1^2 + \epsilon_1^2}}, \tag{30}$$

$$\dot{\hat{\boldsymbol{\eta}}}_1 = \mu_1 z_1 \boldsymbol{\varphi}_1 - l_1 \mu_1 \hat{\boldsymbol{\eta}}_1, \hat{\boldsymbol{\eta}}_1(0) = 0, \tag{31}$$

$$\dot{\hat{\rho}}_1 = \mu_2 |z_1| - l_2 \mu_2 \hat{\rho}_1, \hat{\rho}_1(0) = 0, \tag{32}$$

where $\varrho_1 > 0$, $0.5 < F < 1$, $\epsilon_1 > 0$, $\mu_1 > 0$, $\mu_2 > 0$, $l_1 > 0$ and $l_2 > 0$ are design parameters, and $\hat{\rho}_1$ is used to estimate $\rho_1 := \sup(\frac{|\Delta_1(t)|}{a_1})$.

By using Lemma 2 and substituting (30) into (29), we have

$$\begin{aligned} \dot{V}_1 &\le -\frac{\varrho_1}{2^F} z_1^{2F} + z_1 z_2 + z_1 \tilde{\boldsymbol{\eta}}_1^T \boldsymbol{\varphi}_1 + |z_1|\rho_1 - \frac{\hat{\rho}_1^2 z_1^2}{\sqrt{z_1^2 \hat{\rho}_1^2 + \epsilon_1^2}} \\ &\le -\frac{\varrho_1}{2^F} z_1^{2F} + z_1 z_2 + z_1 \tilde{\boldsymbol{\eta}}_1^T \boldsymbol{\varphi}_1 + |z_1|\tilde{\rho}_1 + \Upsilon \epsilon_1, \end{aligned} \tag{33}$$

where $\tilde{\boldsymbol{\eta}}_1 = \boldsymbol{\eta}_1 - \hat{\boldsymbol{\eta}}_1$, $\tilde{\rho}_1 = \rho_1 - \hat{\rho}_1$, and the definition of Υ is given in Lemma 2. The time derivative of $V_2 = \frac{1}{2} z_2^2$ is

$$\dot{V}_2 = z_2(z_3 + \alpha_2 - \dot{\alpha}_1). \tag{34}$$

To mitigate the difficulty in derivative calculation, a tracking differentiator is introduced to approximate $\dot{\alpha}_1$ as follows:

$$\begin{cases} \dot{\chi}_1 = \chi_2 \\ \lambda_0^2 \dot{\chi}_2 = -\text{sat}_{\epsilon_b}\big(\text{sign}(\phi_\alpha(\chi_1, \alpha_1, \lambda_0 \chi_2))|\phi_\alpha(\chi_1, \alpha_1, \\ \qquad \lambda_0 \chi_2)|^{\lambda_2}\big) - \text{sat}_{\epsilon_b}\big(\text{sign}(\chi_2)|\lambda_0 \chi_2)|^{\mu}\big), \end{cases}$$

in which $0 < \lambda_0 < 1$, $0 < \mu < 1$, $\lambda_1 = \frac{\mu}{2-\mu}$. By Lemma 3, we can see that there exists $\lambda_2 > \frac{2}{\lambda_1}$, such that

$$\chi_2 - \dot{\alpha}_1 = O(\lambda_0^{\lambda_1 \lambda_2 - 1}) \tag{35}$$

can be determined in a finite time.

It follows from (34) that

$$\dot{V}_2 = z_2(z_3 + \alpha_2 - \chi_2 + O(\lambda_0^{\lambda_1 \lambda_2 - 1}). \tag{36}$$

Based on (36), the virtual control law is designed as

$$\alpha_2 = \chi_2 - \frac{\varrho_2}{2^F} z_2^{2F-1} - z_1 - \frac{1}{2} z_2, \tag{37}$$

where $\varrho_2 > 0$, the value of F is the same as that in (30). Substituting (37) into (34) yields

$$\begin{aligned} \dot{V}_2 &\le -z_1 z_2 + z_2 z_3 - \frac{\varrho_2}{2^F} z_2^{2F} + z_2 O(\lambda_0^{\lambda_1 \lambda_2 - 1}) - \frac{1}{2} z_2^2 \\ &\le -z_1 z_2 + z_2 z_3 - \frac{\varrho_2}{2^F} z_2^{2F} + \frac{1}{2} O(\lambda_0^{2\lambda_1 \lambda_2 - 2}). \end{aligned} \tag{38}$$

Define

$$V_3 = \frac{1}{2b_1 \rho_f} z_3^2. \tag{39}$$

Taking the derivative of V_3 with respect to time yields

$$\dot{V}_3 = z_3(\frac{\delta}{\rho_f} + \frac{b_2}{b_1 \rho_f}(x_2 - x_1) + \frac{b_3}{b_1 \rho_f} x_3 + \frac{\Delta_2(t)}{b_1 \rho_f} - \frac{\dot{\alpha}_2}{b_1 \rho_f}). \tag{40}$$

Similar to (35), we can construct the following differentiator

$$\begin{cases} \dot{\chi}_3 = \chi_4 \\ \lambda_0^2 \dot{\chi}_4 = -\text{sat}_{\epsilon_b}\big(\text{sign}(\phi_\alpha(\chi_1, \alpha_2, \lambda_0 \chi_2))|\phi_\alpha(\chi_1, \alpha_2, \\ \qquad \lambda_0 \chi_2)|^{\lambda_2}\big) - \text{sat}_{\epsilon_b}\big(\text{sign}(\chi_2)|\lambda_0 \chi_2)|^{\mu}\big), \end{cases}$$

such that

$$\chi_4 - \dot{\alpha}_2 = O(\lambda_0^{\lambda_1\lambda_2-1}) \tag{41}$$

can be determined in a finite time. With this in mind, it follows from (27) and (40) that

$$\begin{aligned}\dot{V}_3 &= z_3(\frac{\delta}{\rho_f} + \frac{b_2}{b_1\rho_f}(x_2 - x_1) + \frac{b_3}{b_1\rho_f}x_3 + \frac{\Delta_2(t)}{b_1\rho_f} - \frac{\dot{\alpha}_2}{b_1\rho_f}) \\ &= z_3[u_d + (\hat{\boldsymbol{\varpi}} - \boldsymbol{\varpi})^T\hat{\boldsymbol{\omega}} + d_u + \frac{\phi_f}{\rho_f} + \frac{b_2}{b_1\rho_f}(x_2 - x_1) \\ &+ \frac{b_3}{b_1\rho_f}x_3 + \frac{\Delta_2(t)}{b_1\rho_f} + \frac{1}{b_1\rho_f}(-\chi_4 + O(\lambda_0^{\lambda_1\lambda_2-1}))] \\ &\le z_3(u_d + (\hat{\boldsymbol{\varpi}} - \boldsymbol{\varpi})^T\hat{\boldsymbol{\omega}} + \boldsymbol{\eta}_2^T\boldsymbol{\omega}_2) + |z_3|\rho_2,\end{aligned} \tag{42}$$

where $\boldsymbol{\eta}_2 = [\frac{b_2}{b_1\rho_f}, \frac{b_3}{b_1\rho_f}, \frac{-1}{b_1\rho_f}]^T, \boldsymbol{\varphi}_2 = [x_2 - x_1, x_3, \chi_4]^T$, $\rho_2 := \sup(d_u + \frac{\phi_f}{\rho_f} + \frac{\Delta_2(t)}{b_1\rho_f} + \frac{O(\lambda_0^{\lambda_1\lambda_2-1})}{b_1\rho_f})$.

In view of (42), we design

$$u_d = -\frac{\varrho_3}{2^F}z_3^{2F-1} - z_2 - \frac{1}{2}z_3 - \hat{\boldsymbol{\eta}}_2^T\boldsymbol{\varphi}_2 - \frac{\hat{\rho}_2^2 z_3}{\sqrt{z_3^2\hat{\rho}_2^2 + \epsilon_2^2}}, \tag{43}$$

in which

$$\dot{\hat{\boldsymbol{\eta}}}_2 = \mu_3 z_3\boldsymbol{\varphi}_2 - l_3\mu_3\hat{\boldsymbol{\eta}}_2, \hat{\boldsymbol{\eta}}_2(0) = 0, \tag{44}$$

$$\dot{\hat{\rho}}_2 = \mu_4|z_3| - l_4\mu_4\hat{\rho}_2, \hat{\rho}_2(0) = 0, \tag{45}$$

where $\varrho_3 > 0$, $\epsilon_2 > 0$, $\mu_3 > 0, \mu_4 > 0, l_3 > 0$ and $l_4 > 0$ are design parameters, and $\hat{\rho}_2$ is used to estimate ρ_2. Substituting (43) into (42), we get

$$\begin{aligned}\dot{V}_3 \le &-\frac{\varrho_3}{2^F}z_3^{2F} - z_2z_3 + z_3(\hat{\boldsymbol{\varpi}} - \boldsymbol{\varpi})^T\hat{\boldsymbol{\omega}} + z_3\tilde{\boldsymbol{\eta}}_2^T\boldsymbol{\omega}_2 \\ &+ |z_3|\tilde{\rho}_2 + \Upsilon\epsilon_2,\end{aligned} \tag{46}$$

where $\tilde{\boldsymbol{\eta}}_2 = \boldsymbol{\eta}_2 - \hat{\boldsymbol{\eta}}_2$, $\tilde{\rho}_2 = \rho_2 - \hat{\rho}_2$.

To ensure the estimates $\hat{m}_r(t)) \ge m_{r0}$ and $\hat{m}_l(t) \ge m_{l0}$, the dead-zone parameter update law is designed as follows:

$$\dot{\hat{\boldsymbol{\varpi}}} = \mathrm{Proj}_{\underline{\varpi},\overline{\varpi}}(-\mu_5 z_3\hat{\boldsymbol{\omega}} - l_5\mu_5\hat{\boldsymbol{\varpi}}), \tag{47}$$

where $\underline{\varpi} \in \mathbb{R}, \overline{\varpi} \in \mathbb{R}, \underline{\varpi} < \overline{\varpi}$\$, $\mathrm{Proj}_{\underline{\varpi},\overline{\varpi}}(\cdot)$ is a projection operator. For $\boldsymbol{\tau} = [\tau_1, \tau_2, \tau_3, \tau_4]^T \in \mathbb{R}^4$, $\mathrm{Proj}_{\underline{\varpi},\overline{\varpi}}(\boldsymbol{\tau}) \triangleq [\mathrm{proj}_{\underline{\varpi},\overline{\varpi}}(\tau_1), \mathrm{proj}_{\underline{\varpi},\overline{\varpi}}(\tau_2), \mathrm{proj}_{\underline{\varpi},\overline{\varpi}}(\tau_3), \mathrm{proj}_{\underline{\varpi},\overline{\varpi}}(\tau_4)]^T$, where

$$\mathrm{proj}_{\underline{\varpi},\overline{\varpi}}(\tau_i) = \begin{cases} 0, & \text{if } \hat{\varpi}_i = \underline{\varpi} \text{ and } \tau_i \le 0 \\ 0, & \text{if } \hat{\varpi}_i = \overline{\varpi} \text{ and } \tau_i \ge 0 \\ \tau_i, & \text{otherwise} \end{cases} \tag{48}$$

with $i = 1, 2, 3, 4$. This projection operator satisfies the following property:

$$-\tilde{\boldsymbol{\varpi}}^T\mathrm{Proj}(\boldsymbol{\tau}) \le -\tilde{\boldsymbol{\varpi}}^T\boldsymbol{\tau}. \tag{49}$$

Remark 2: In this paper, two finite-time differentiators are used to estimate the derivatives of virtual control signals, such that the inherent differential explosion in backstepping control is avoided.

Remark 3: For the design parameters $\wp$ in (24), ϱ_1, ϵ_1, μ_1, μ_2, l_1 and l_2 in (30)-(32), ϱ_2, in (37), ϱ_3, ϵ_2, μ_3, μ_4, l_3 and l_4 in (43)-(45), μ_5 and l_5 in (47), it is difficult to determine the optimal values theoretically. Their recommended value ranges are as follows: $\wp \in [0.1, 1]$, $\varrho_1 \in [5, 10]$, $\varrho_2 \in [5, 10]$, $\varrho_3 \in [5, 10]$, $\epsilon_1 \in [0.001, 0.1]$, $\epsilon_2 \in [0.001, 0.1]$, $\mu_1 \in [0.5, 10]$, $\mu_2 \in [0.05, 0.5]$, $\mu_3 \in [0.5, 10]$, $\mu_4 \in [0.05, 0.5]$, $\mu_5 \in [0.1, 5]$, $l_1 \in [0.01, 0.1]$, $l_2 \in [0.01, 0.1]$, $l_3 \in [0.01, 0.1]$, $l_4 \in [0.01, 0.1]$ and $l_5 \in [0.01, 0.1]$.

C. STABILITY ANALYSIS

Theorem 1: Consider the closed-loop flight-path tracking control system (7) under Assumption 1, with the control law (23) and (43), the virtual control signals (30) and (37), tracking differentiators (35) and (41), and the adaptive laws (31), (32), (44), (45) and (47). Then, practical finite-time tracking performance can be guaranteed, while all closed-loop signals are uniformly bounded.

Proof: Construct a Lyapunov function as follows:

$$V_\sigma = V_{1\sigma} + V_2 + V_{3\sigma}, \tag{50}$$

where

$$V_{1\sigma} = V_1 + \frac{1}{2\mu_1}\tilde{\boldsymbol{\eta}}_1^T\tilde{\boldsymbol{\eta}}_1 + \frac{1}{2\mu_2}\tilde{\rho}_1^2 \tag{51}$$

and

$$V_{3\sigma} = V_3 + \frac{1}{2\mu_3}\tilde{\boldsymbol{\eta}}_2^T\tilde{\boldsymbol{\eta}}_2 + \frac{1}{2\mu_4}\tilde{\rho}_2^2 + \frac{1}{2\mu_5}\tilde{\boldsymbol{\varpi}}^T\tilde{\boldsymbol{\varpi}}. \tag{52}$$

By using (33), we get

$$\begin{aligned}\dot{V}_{1\sigma} \le &-\frac{\varrho_1}{2^F}z_1^{2F} + z_1z_2 + z_1\tilde{\boldsymbol{\eta}}_1^T\boldsymbol{\varphi}_1 + |z_1|\tilde{\rho}_1 + \Upsilon\epsilon_1 \\ &- \frac{1}{\mu_1}\tilde{\boldsymbol{\eta}}_1^T\dot{\hat{\boldsymbol{\eta}}}_1 - \frac{1}{\mu_2}\tilde{\rho}_1\dot{\hat{\rho}}_1.\end{aligned} \tag{53}$$

It follows from (31) that

$$\begin{aligned}z_1\tilde{\boldsymbol{\eta}}_1^T\boldsymbol{\varphi}_1 - \frac{1}{\mu_1}\tilde{\boldsymbol{\eta}}_1^T\dot{\hat{\boldsymbol{\eta}}}_1 &= z_1\tilde{\boldsymbol{\eta}}_1^T\boldsymbol{\varphi}_1 - \frac{1}{\mu_1}\tilde{\boldsymbol{\eta}}_1^T(\mu_1 z_1\boldsymbol{\varphi}_1 - l_1\mu_1\hat{\boldsymbol{\eta}}_1) \\ &\le -\frac{l_1}{2}\tilde{\boldsymbol{\eta}}_1^T\tilde{\boldsymbol{\eta}}_1 + \frac{l_1}{2}\boldsymbol{\eta}_1^T\boldsymbol{\eta}_1.\end{aligned} \tag{54}$$

Invoking (32), we obtain

$$\begin{aligned}|z_1|\tilde{\rho}_1 - \frac{1}{\mu_2}\tilde{\rho}_1\dot{\hat{\rho}}_1 &= |z_1|\tilde{\rho}_1 - \frac{1}{\mu_2}\tilde{\rho}_1(\mu_2|z_1| - l_2\mu_2\hat{\rho}_1) \\ &\le -\frac{l_2}{2}\tilde{\rho}_1^2 + \frac{l_2}{2}\rho_1^2.\end{aligned} \tag{55}$$

From the above three inequalities, we obtain

$$\begin{aligned}\dot{V}_{1\sigma} \le &-\frac{\varrho_1}{2^F}z_1^{2F} + z_1z_2 - \frac{l_1}{2}\tilde{\boldsymbol{\eta}}_1^T\tilde{\boldsymbol{\eta}}_1 + \frac{l_1}{2}\boldsymbol{\eta}_1^T\boldsymbol{\eta}_1 - \frac{l_2}{2}\tilde{\rho}_1^2 \\ &+ \frac{l_2}{2}\rho_1^2 + \Upsilon\epsilon_1.\end{aligned} \tag{56}$$

Combining (38) with (56), we have

$$\begin{aligned}\dot{V}_{1\sigma} + \dot{V}_2 \le &-\frac{\varrho_1}{2^F}z_1^{2F} - \frac{\varrho_2}{2^F}z_2^{2F} - \frac{l_1}{2}\tilde{\boldsymbol{\eta}}_1^T\tilde{\boldsymbol{\eta}}_1 - \frac{l_2}{2}\tilde{\rho}_1^2 + \frac{l_1}{2}\boldsymbol{\eta}_1^T\boldsymbol{\eta}_1 \\ &+ \frac{l_2}{2}\rho_1^2 + \Upsilon\epsilon_1 + \frac{1}{2}O(\lambda_0^{2\lambda_1\lambda_2-2}) + z_2z_3.\end{aligned} \tag{57}$$

Invoking (46) and (52), we have

$$\dot{V}_{3\sigma} \leq -\frac{\varrho_3}{2^F} z_3^{2F} - z_2 z_3 - z_3 \tilde{\boldsymbol{\varpi}}^T \hat{\boldsymbol{\omega}} + z_3 \tilde{\boldsymbol{\eta}}_2^T \boldsymbol{\omega}_2 + |z_3|\tilde{\rho}_2 + \epsilon_2 - \frac{1}{\mu_5} \tilde{\boldsymbol{\varpi}}^T \dot{\hat{\boldsymbol{\varpi}}} - \frac{1}{\mu_3} \tilde{\boldsymbol{\eta}}_2^T \dot{\hat{\boldsymbol{\eta}}}_2 - \frac{1}{\mu_4} \tilde{\rho}_2 \dot{\hat{\rho}}_2. \tag{58}$$

Similar to (55), it can be inferred from (44) and (45) that

$$z_3 \tilde{\boldsymbol{\eta}}_2^T \boldsymbol{\varphi}_2 - \frac{1}{\mu_3} \tilde{\boldsymbol{\eta}}_2^T \dot{\hat{\boldsymbol{\eta}}}_3 = z_3 \tilde{\boldsymbol{\eta}}_2^T \boldsymbol{\varphi}_2 - \frac{1}{\mu_3} \tilde{\boldsymbol{\eta}}_2^T (\mu_3 z_3 \boldsymbol{\varphi}_3 - l_3 \mu_3 \hat{\boldsymbol{\eta}}_2) \leq -\frac{l_3}{2} \tilde{\boldsymbol{\eta}}_2^T \tilde{\boldsymbol{\eta}}_2 + \frac{l_3}{2} \boldsymbol{\eta}_2^T \boldsymbol{\eta}_2 \tag{59}$$

and

$$|z_3|\tilde{\rho}_2 - \frac{1}{\mu_4} \tilde{\rho}_2 \dot{\hat{\rho}}_2 = |z_3|\tilde{\rho}_2 - \frac{1}{\mu_4} \tilde{\rho}_2 (\mu_4 |z_3| - l_4 \mu_4 \hat{\rho}_2) \leq -\frac{l_4}{2} \tilde{\rho}_2^2 + \frac{l_4}{2} \rho_2^2. \tag{60}$$

It follows from (47) that

$$\begin{aligned} &- z_3 \tilde{\boldsymbol{\varpi}}^T \hat{\boldsymbol{\omega}} - \frac{1}{\mu_5} \tilde{\boldsymbol{\varpi}}^T \dot{\hat{\boldsymbol{\varpi}}} \\ &= -z_3 \tilde{\boldsymbol{\varpi}}^T \hat{\boldsymbol{\omega}} - \frac{1}{\mu_5} \tilde{\boldsymbol{\varpi}}^T \mathrm{Proj}(-\mu_5 z_3 \hat{\boldsymbol{\omega}} - l_5 \mu_5 \hat{\boldsymbol{\varpi}}). \end{aligned} \tag{61}$$

According to the property (49), from (61), we can get

$$\begin{aligned} &- z_3 \tilde{\boldsymbol{\varpi}}^T \hat{\boldsymbol{\omega}} - \frac{1}{\mu_5} \tilde{\boldsymbol{\varpi}}^T \dot{\hat{\boldsymbol{\varpi}}} \\ &\leq -z_3 \tilde{\boldsymbol{\varpi}}^T \hat{\boldsymbol{\omega}} - \frac{1}{\mu_5} \tilde{\boldsymbol{\varpi}}^T (-\mu_5 z_3 \hat{\boldsymbol{\omega}} - l_5 \mu_5 \hat{\boldsymbol{\varpi}}) \\ &\leq -\frac{l_5}{2} \tilde{\boldsymbol{\varpi}}^T \tilde{\boldsymbol{\varpi}} + \frac{l_5}{2} \boldsymbol{\varpi}^T \boldsymbol{\varpi}. \end{aligned} \tag{62}$$

Combining (58) -(60) with (62), we obtain

$$\dot{V}_{3\sigma} \leq -\frac{\varrho_3}{2^F} z_3^{2F} - z_2 z_3 - \frac{l_5}{2} \tilde{\boldsymbol{\varpi}}^T \tilde{\boldsymbol{\varpi}} - \frac{l_3}{2} \tilde{\boldsymbol{\eta}}_2^T \tilde{\boldsymbol{\eta}}_2 - \frac{l_4}{2} \tilde{\rho}_2^2 + \frac{l_5}{2} \boldsymbol{\varpi}^T \boldsymbol{\varpi} + \frac{l_3}{2} \boldsymbol{\eta}_2^T \boldsymbol{\eta}_2 + \frac{l_4}{2} \rho_2^2 + \epsilon_2. \tag{63}$$

From (57) and (63), we get

$$\begin{aligned} \dot{V}_\sigma \leq &-\frac{\varrho_1}{2^F} z_1^{2F} - \frac{\varrho_2}{2^F} z_2^{2F} - \frac{\varrho_3}{2^F} z_3^{2F} - \frac{l_1}{2} \tilde{\boldsymbol{\eta}}_1^T \tilde{\boldsymbol{\eta}}_1 - \frac{l_2}{2} \tilde{\rho}_1^2 \\ &- \frac{l_3}{2} \tilde{\boldsymbol{\eta}}_2^T \tilde{\boldsymbol{\eta}}_2 - \frac{l_4}{2} \tilde{\rho}_2^2 - \frac{l_5}{2} \tilde{\boldsymbol{\varpi}}^T \tilde{\boldsymbol{\varpi}} + \frac{l_1}{2} \boldsymbol{\eta}_1^T \boldsymbol{\eta}_1 + \frac{l_2}{2} \rho_1^2 \\ &+ \frac{l_3}{2} \boldsymbol{\eta}_2^T \boldsymbol{\eta}_2 + \frac{l_4}{2} \rho_2^2 + \frac{l_5}{2} \boldsymbol{\varpi}^T \boldsymbol{\varpi} + \epsilon_2 + \epsilon_1 \\ &+ \frac{1}{2} O(\lambda_0^{2\lambda_1 \lambda_2 - 2}). \end{aligned} \tag{64}$$

By Lemma 4, the following five inequalities hold:

$$\begin{aligned} -\frac{l_1}{2} \tilde{\boldsymbol{\eta}}_1^T \tilde{\boldsymbol{\eta}}_1 &\leq -(\frac{l_1}{2} \tilde{\boldsymbol{\eta}}_1^T \tilde{\boldsymbol{\eta}}_1)^F + (1-F) F^{\frac{F}{1-F}}, \\ &= -(l_1 \mu_1)^F (\frac{1}{2\mu_1} \tilde{\boldsymbol{\eta}}_1^T \tilde{\boldsymbol{\eta}}_1)^F + (1-F) F^{\frac{F}{1-F}}, \end{aligned} \tag{65}$$

$$\begin{aligned} -\frac{l_2}{2} \tilde{\rho}_1^2 &\leq -(\frac{l_2}{2} \tilde{\rho}_1^2)^F + (1-F) F^{\frac{F}{1-F}} \\ &= -(l_2 \mu_2)^F (\frac{1}{2\mu_2} \tilde{\rho}_1^2)^F + (1-F) F^{\frac{F}{1-F}}, \end{aligned} \tag{66}$$

$$\begin{aligned} -\frac{l_3}{2} \tilde{\boldsymbol{\eta}}_2^T \tilde{\boldsymbol{\eta}}_2 &\leq -(\frac{l_3}{2} \tilde{\boldsymbol{\eta}}_2^T \tilde{\boldsymbol{\eta}}_2)^F + (1-F) F^{\frac{F}{1-F}}, \\ &= -(l_3 \mu_3)^F ((\frac{1}{2\mu_3} \tilde{\boldsymbol{\eta}}_2^T \tilde{\boldsymbol{\eta}}_2)^F + (1-F) F^{\frac{F}{1-F}}, \end{aligned} \tag{67}$$

$$\begin{aligned} -\frac{l_4}{2} \tilde{\rho}_2^2 &\leq -(\frac{l_4}{2} \tilde{\rho}_2^2)^F + (1-F) F^{\frac{F}{1-F}}, \\ &= -(l_4 \mu_4)^F (\frac{1}{2\mu_4} \tilde{\rho}_2^2)^F + (1-F) F^{\frac{F}{1-F}}, \end{aligned} \tag{68}$$

$$\begin{aligned} -\frac{l_5}{2} \tilde{\boldsymbol{\varpi}}^T \tilde{\boldsymbol{\varpi}} &\leq -(\frac{l_5}{2} \tilde{\boldsymbol{\varpi}}^T \tilde{\boldsymbol{\varpi}})^F + (1-F) F^{\frac{F}{1-F}} \\ &= -(l_5 \mu_5)^F (\frac{1}{2\mu_5} \tilde{\boldsymbol{\varpi}}^T \tilde{\boldsymbol{\varpi}})^F + (1-F) F^{\frac{F}{1-F}}. \end{aligned} \tag{69}$$

Substituting (65)-(69) into (64) leads to

$$\begin{aligned} \dot{V}_\sigma \leq &-\frac{\varrho_1}{2^F} z_1^{2F} - \frac{\varrho_2}{2^F} z_2^{2F} - \frac{\varrho_3}{2^F} z_3^{2F} - (l_1 \mu_1)^F (\frac{1}{2\mu_1} \tilde{\boldsymbol{\eta}}_1^T \tilde{\boldsymbol{\eta}}_1)^F \\ &- (l_2 \mu_2)^F (\frac{1}{2\mu_2} \tilde{\rho}_1^2)^F - (l_3 \mu_3)^F (\frac{1}{2\mu_3} \tilde{\boldsymbol{\eta}}_2^T \tilde{\boldsymbol{\eta}}_2)^F \\ &- (l_4 \mu_4)^F (\frac{1}{2\mu_4} \tilde{\rho}_2^2)^F - (l_5 \mu_5)^F (\frac{1}{2\mu_5} \tilde{\boldsymbol{\varpi}}^T \tilde{\boldsymbol{\varpi}})^F + \zeta \\ \leq &-\bar{\varrho} \Big[(\frac{1}{2} z_1^2)^F + (\frac{1}{2} z_2^2)^F + (\frac{1}{2} z_3^2)^F + (\frac{1}{2\mu_1} \tilde{\boldsymbol{\eta}}_1^T \tilde{\boldsymbol{\eta}}_1)^F \\ &+ (\frac{1}{2\mu_2} \tilde{\rho}_1^2)^F + (\frac{1}{2\mu_3} \tilde{\boldsymbol{\eta}}_2^T \tilde{\boldsymbol{\eta}}_2)^F + (\frac{1}{2\mu_4} \tilde{\rho}_2^2)^F \\ &+ (\frac{1}{2\mu_5} \tilde{\boldsymbol{\varpi}}^T \tilde{\boldsymbol{\varpi}})^F \Big] + \zeta_\rho, \end{aligned} \tag{70}$$

where $\zeta_\rho = 5(1-F) F^{\frac{F}{1-F}} + \frac{l_1}{2} \boldsymbol{\eta}_1^T \boldsymbol{\eta}_1 + \frac{l_2}{2} \rho_1^2 + \frac{l_3}{2} \boldsymbol{\eta}_2^T \boldsymbol{\eta}_2 + \frac{l_4}{2} \rho_2^2 + \frac{l_5}{2} \boldsymbol{\varpi}^T \boldsymbol{\varpi} + \epsilon_2 + \epsilon_1 + \frac{1}{2} O(\lambda_0^{2\lambda_1 \lambda_2 - 2})$, and $\bar{\varrho} := \min(\varrho_1, \varrho_2, \varrho_3, (l_i \mu_i)^F)$, $i = 1, 2, \cdots, 5$.

By Lemma 5, it follows from (70) that

$$\dot{V}_\sigma \leq -\bar{\varrho} V_\sigma^F + \zeta_\rho. \tag{71}$$

According to Lemma 1, it can be inferred from (71) that $V^F \leq \frac{\zeta_\rho}{\bar{\varrho}(1-c_0)}$ holds for $t \geq t_r$ where $t_r = \frac{1}{(1-F)\bar{\varrho} c_0} [V^{1-F} - \frac{\zeta_\rho}{\bar{\varrho}(1-c_0)}^{\frac{1-F}{F}}]$, and the denotation of c_0 can be seen in Lemma 1. Further, we have

$$|z_1(t)| \leq 2(\frac{\zeta_\rho}{\bar{\varrho}(1-c_0)})^{\frac{1}{2F}}, \forall t \geq t_r. \tag{72}$$

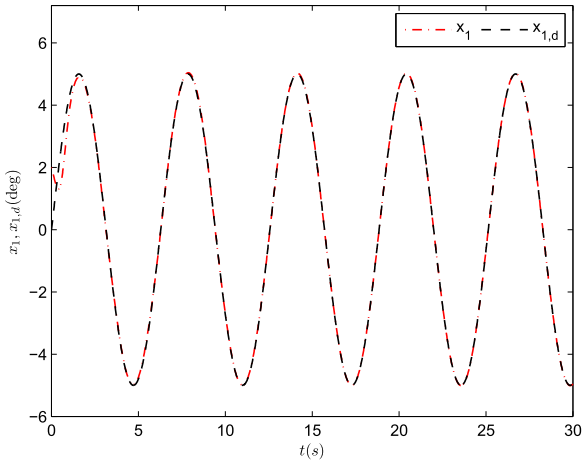

FIGURE 4. Tracking result of flight path angle (RAFFFAC).

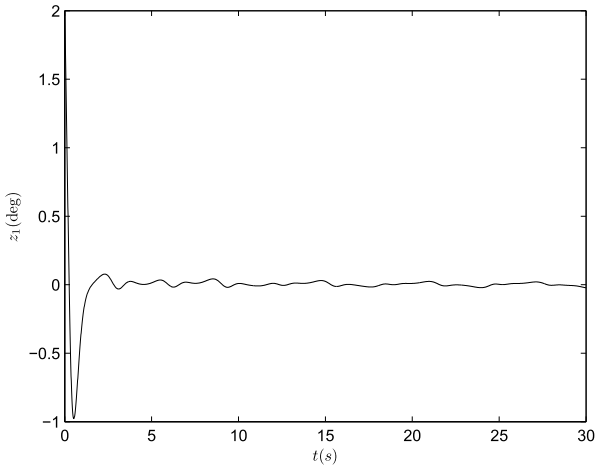

FIGURE 5. Tracking error (RAFFFAC).

These results demonstrate that the closed-loop flight-path tracking control system (7) is a SGPFS system, and the tracking error falls in a small neighborhood of the origin during a finite time.

On another hand, it follows from (71) that $z_1, z_2, z_3, \hat{\rho}_1, \hat{\rho}_2$ and $\hat{\boldsymbol{\varpi}}$ are guaranteed to be bounded. On basis of this, the boundedness of $\alpha_1, \alpha_2, u_d, v$, and δ can be achieved from (30), (37), (25), (23) and (27). Further, the boundedness of all other signals can be obtained. ■

In this study, both unknown deadzone nonlinearity and actuator faults are considered during controller design. In the process of controller design, no sliding mode surface is constructed for accomplishing controller design, which simplifies the control system design.

IV. ILLUSTRATIVE EXAMPLE

In this section, the numerical simulation results are presented to show the performance of the proposed control scheme. The control objective is to make the state x_1 track the command flight path angle $x_{1,d} = 5^\circ \sin(t)$. The actual parameter values are $\bar{L}_o = 0.1, \bar{L}_\alpha = 1.0, M_\alpha = 0.1, M_q = -0.02, M_\delta = 1.0$, the actuator faults are $\rho_f = 0.8$ and ϕ_f is a random number in the range of $[-0.5, 0.5]$, and the true parameters of the deadzone are $b_r = 0.5, b_l = -0.6, m_r = 1, m_l = 1.5$ and $\Delta_1(t) = 0.01\sin(2t), \Delta_2(t) = 0.05\cos(2t)$, which are not needed to be known durign controller design.

The robust adaptive fault-tolerant finite-time flight-path angle control (RAFFFAC) law (23) and (43), the virtual control signals (30) and (37), tracking differentiators (35) and (41), and the adaptive laws (31), (32), (44), (45) and (47) are used for simulation, taking $\digamma = 97/100, \epsilon_1 = 0.01, \epsilon_2 = 0.01, \mu_1 = 1, \mu_2 = 0.1, \mu_3 = 1, \mu_4 = 0.1, \mu_5 = 0.5, l_1 = l_2 = l_3 = l_4 = l_5 = 0.1, \varrho_1 = 5, \varrho_2 = 5, \varrho_3 = 5, \underline{\varpi} = 0.2, \overline{\varpi} = 10, \wp = 0.5$. The initial values are chosen as follows: $x_1(0) = 2, x_2(0) = 0, x_3(0) = 0$. The simulation results are shown in Figs. 4-7. Fig. 4 shows the system output curve and the reference trajectory curve for the case of using RAFFFAC law. The tracking error is plotted in Fig. 5. The curve of pitch angle is depicted in Fig. 6. Fig. 7 displays the control input curve under the action of RAFFFAC law.

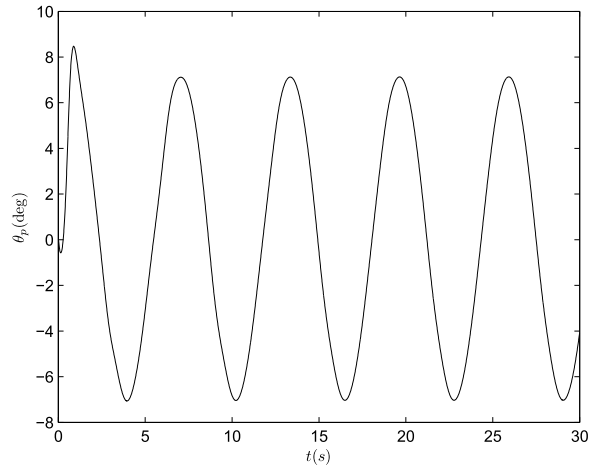

FIGURE 6. Angle of pitch (RAFFFAC).

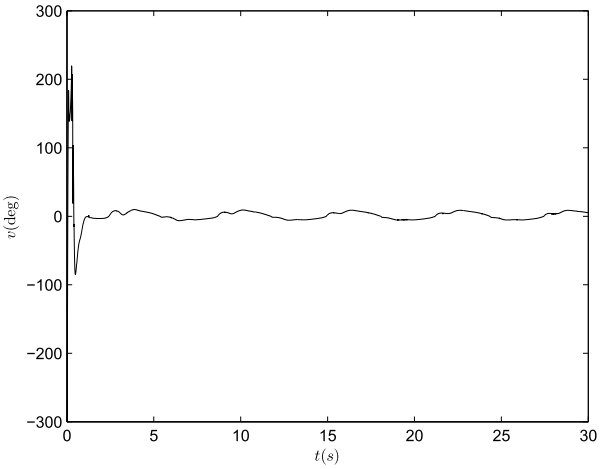

FIGURE 7. Control input (RAFFFAC).

To further demonstrate the advantage of our proposed control scheme, two other control algorithms are adopted for comparison.

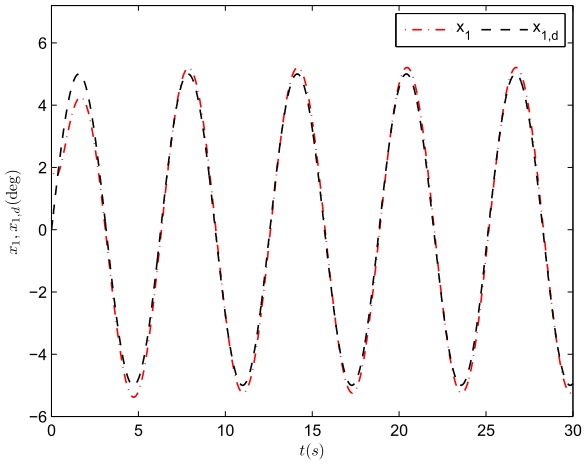

FIGURE 8. x_1 and $x_{1,d}$ (PIDC).

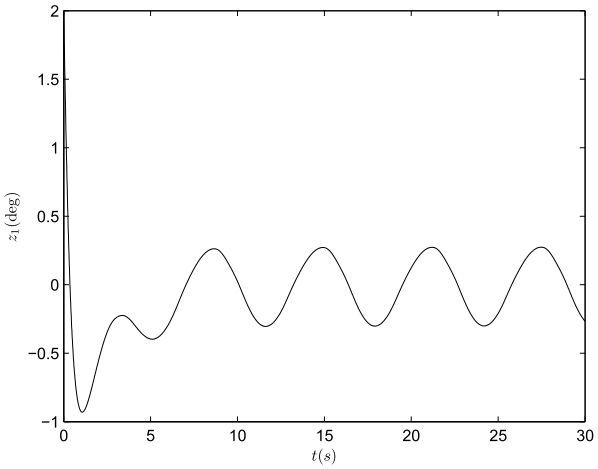

FIGURE 9. Tracking error(PIDC).

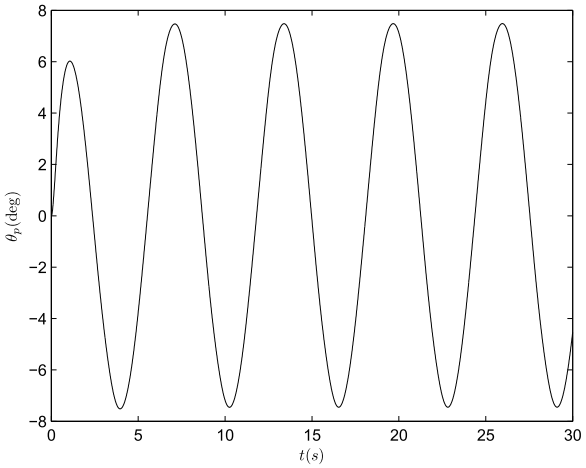

FIGURE 10. Angle of pitch (PIDC).

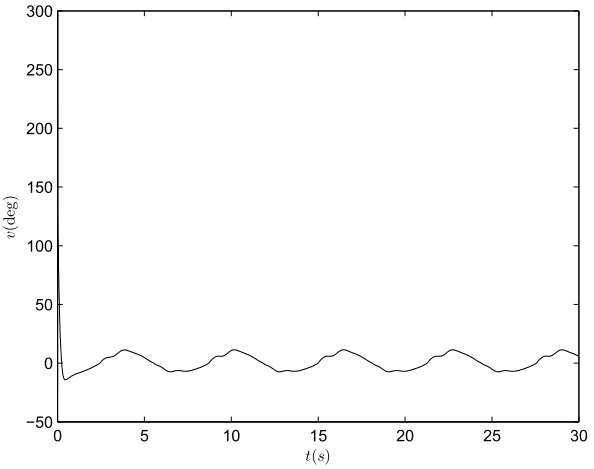

FIGURE 11. Control input (PIDC).

PIDC). A traditional PID control (PIDC) law is introduced as follows:

$$v = k_p(x_{1,d} - x_1) + k_i \int_0^t (x_{1,d}(\tau) - x_1(\tau))d\tau + k_d(\dot{x}_{1,d} - \dot{x}_1), \tag{73}$$

where the design parameters are chosen as $k_p = 11, k_i = 0.3, k_d = 21$.

ADSC). An adaptive dynamic surface control(ADSC) law is given in [3] to solve the flight-path angle control problem for aircraft systems with neither actuator deadzone nor actuator fault as follows:

$$v = \hat{\boldsymbol{\theta}}_b^T \boldsymbol{\varphi}_b, \tag{74}$$

where $\boldsymbol{\varphi}_b = [x_2 - x_1, x_3, \frac{\rho_b^2 S_3}{2\varepsilon_b} - \dot{x}_{3,d} + c_c S_3]^T, \dot{\hat{\boldsymbol{\theta}}}_b = \Gamma_b \boldsymbol{\varphi}_b S_3 - \eta_b \Gamma_b \hat{\boldsymbol{\theta}}_b, S_3 = x_3 - x_{3,d}$. The signal $x_{3,d}$ is available from the following filtering operation:

$$\tau_3 \dot{x}_{3,d} + x_{3,d} = \dot{x}_{2,d} - c_b S_2, \tag{75}$$

where $S_2 = x_2 - x_{2,d}$, and the signal $x_{2,d}$ is available from the following filtering operation:

$$\tau_2 \dot{x}_{2,d} + x_{2,d} = \hat{\boldsymbol{\theta}}_a^T \boldsymbol{\varphi}_a + x_1, \tag{76}$$

in which $\boldsymbol{\varphi}_a = [1, -\cos x_1, \frac{\rho_a^2 S_1}{2\varepsilon_a} - \dot{x}_{1,d} + c_a S_1]^T, \dot{\hat{\boldsymbol{\theta}}}_a = \Gamma_a \boldsymbol{\varphi}_a S_1 - \eta_a \Gamma_a \hat{\boldsymbol{\theta}}_a, S_1 = z_1 = x_1 - x_{1,d}$. In this simulation, the values of parameters are chosen as follows: $c_a = 3, c_b = 3, c_3 = 3, \Gamma_a = \text{diag}(0.5, 0.6, 0.02), \Gamma_b = \text{diag}(0.5, 0.5, 0.1), \eta_a = \eta_b = 0.001, \varepsilon_a = \varepsilon_b = 0.01, \rho_a = \rho_b = 0.1$.

The initial values of PIDC system and ADSC system are chosen to be the same as those of RAFFFAC system. The PIDC simulation results presented in Figs. 8-11 are system output response, tracking error, angle of pitch and control input, respectively. The ADSC simulation results presented in Figs. 12-15 are system output response,tracking error, angle of pitch and control input respectively. From Figs. 5, 8, 12, we can see that x_1 can track the reference trajectory in three control schemes. According to the corresponding tracking errors shown in Figs. 6, 9, 13, we can see that the closed-loop RAFFFAC system possesses the smallest

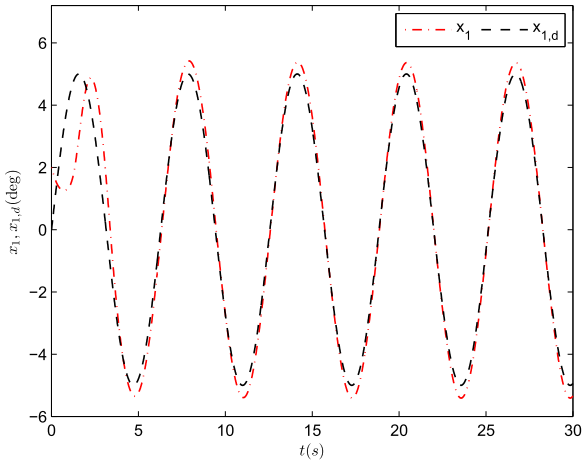

FIGURE 12. x_1 and $x_{1,d}$ (ADSC).

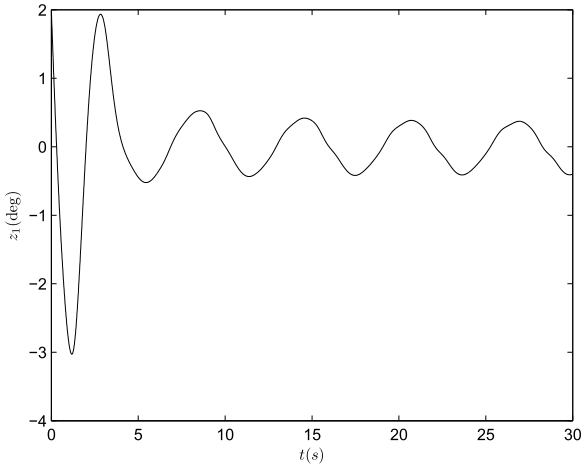

FIGURE 13. Tracking error(ADSC).

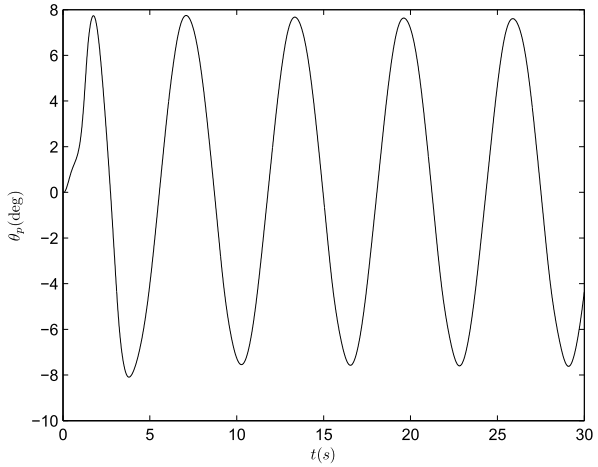

FIGURE 14. Angle of pitch (ADSC).

steady-state position error among three closed-loop control systems.

For further performance comparison, root mean squared error (RMSE) is introduced to measure the performance as

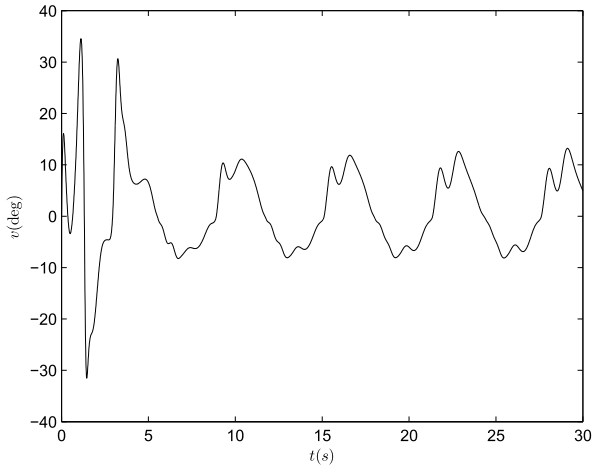

FIGURE 15. Control input (ADSC).

TABLE 1. RSME value comparison.

	RAFFFAC	PIDC	ADSC
RMSE	0.1593	0.3233	0.6752

follows:

$$\text{RMSE} = \sqrt{\frac{1}{n}\sum_{i=1}^{n} z_1^2(t)}, \tag{77}$$

where n denotes the number of samples. The RMSE values of three control algorithms are listed in Table 1, from which we can see that the RMSE value of RAFFFAC is the smallest among the three control schemes. The above results verify the effectiveness of the proposed control scheme.

V. CONCLUSION

To achieve a finite-time flight-path angle-tracking performance of aircraft systems with unknown deadzone and actuator faults, a robust adaptive fault-tolerant finite-time control strategy has been developed. A new smooth deadzone inverse model has been established to compensate for deadzone nonlinearity. During the backstepping control design, two finite-time differentiators are employed to estimate the derivatives of virtual control signals. Simulation results show the effectiveness of our proposed fault-tolerant finite-time flight-Path angle control scheme.

REFERENCES

[1] M. Sharma, "Flight-path angle control via neuro-adaptive backstepping," in *Proc. AIAA Guid., Navigat., Control Conf. Exhibit*, Monterey, CA, USA, Aug. 2002, p. 4451.

[2] L. Duan, W. Lu, F. Mora-Camino, and T. Miquel, "Flight-path tracking control of a transportation aircraft: Comparison of two nonlinear design approaches," in *Proc. IEEE/AIAA 25TH Digit. Avionics Syst. Conf.*, Oct. 2006, pp. 1–9.

[3] Y. Guo and J. Liu, "Adaptive dynamic surface control for aircraft flight path angle," *J. Beijing Univ. Aeronaut. Astronaut.*, vol. 39, no. 2, pp. 275–279, Feb. 2013.

[4] Y. Wei, H. Xu, Y. Xue, Z. Li, and H. Tian, "Flight path angle controller design based on adaptive backstepping terminal sliding mode control method," in *Proc. 9th Asia–Pacific Int. Symp. Aerosp. Technol. (APISAT)*. Singapore: Springer, 2019, pp. 2466–2479.

[5] X. Li, W. Fu, L. Liu, and Y. Wang, "Adaptive dynamic surface control for aircraft with multiple disturbances based on radial basis network," *IEEE Access*, vol. 8, pp. 57709–57721, 2020.

[6] Y. Sun, B. Chen, C. Lin, and H. Wang, "Finite-time adaptive control for a class of nonlinear systems with nonstrict feedback structure," *IEEE Trans. Cybern.*, vol. 48, no. 10, pp. 2774–2782, Oct. 2018.

[7] Y. Pan, W. Ji, H.-K. Lam, and L. Cao, "An improved predefined-time adaptive neural control approach for nonlinear multiagent systems," *IEEE Trans. Autom. Sci. Eng.*, early access, Oct. 20, 2023, doi: 10.1109/TASE.2023.3324397.

[8] S. Yang, Y. Pan, L. Cao, and L. Chen, "Predefined-time fault-tolerant consensus tracking control for multi-UAV systems with prescribed performance and attitude constraints," *IEEE Trans. Aerosp. Electron. Syst.*, early access, Feb. 29, 2024, doi: 10.1109/TAES.2024.3371406.

[9] K. Raj, V. Muthukumar, S. N. Singh, and K. W. Lee, "Finite-time sliding mode and super-twisting control of fighter aircraft," *Aerosp. Sci. Technol.*, vols. 82–83, pp. 487–498, Nov. 2018.

[10] H. Du, W. Zhu, G. Wen, and D. Wu, "Finite-time formation control for a group of quadrotor aircraft," *Aerosp. Sci. Technol.*, vol. 69, pp. 609–616, Oct. 2017.

[11] W. Zhu, H. Du, Y. Cheng, and Z. Chu, "Hovering control for quadrotor aircraft based on finite-time control algorithm," *Nonlinear Dyn.*, vol. 88, no. 4, pp. 2359–2369, Jun. 2017.

[12] J. Liu, M. Sun, Z. Chen, and Q. Sun, "Super-twisting sliding mode control for aircraft at high angle of attack based on finite-time extended state observer," *Nonlinear Dyn.*, vol. 99, no. 4, pp. 2785–2799, Mar. 2020.

[13] H. Du, B. Yu, J. Wei, J. Zhang, D. Wu, and W. Tao, "Attitude trajectory planning and attitude control for quad-rotor aircraft based on finite-time control technique," *Appl. Math. Comput.*, vol. 386, Dec. 2020, Art. no. 125493.

[14] Y. Fu, J. Shi, and Y. Lyu, "Finite-time observer based predefined-time aircraft attitude tracking control," *Int. J. Control, Autom. Syst.*, vol. 21, no. 11, pp. 3757–3766, Nov. 2023.

[15] X. Bu, Q. Qi, and B. Jiang, "A simplified finite-time fuzzy neural controller with prescribed performance applied to waverider aircraft," *IEEE Trans. Fuzzy Syst.*, vol. 30, no. 7, pp. 2529–2537, Jul. 2022.

[16] H. Cheng, W. Fu, C. Dong, Q. Wang, and Y. Hou, "Asynchronously finite-time H_∞ control for morphing aircraft," *Trans. Inst. Meas. Control*, vol. 40, no. 16, pp. 4330–4344, Dec. 2018.

[17] G. Tao and P. V. Kokotovic, "Continuous-time adaptive control of systems with unknown backlash," *IEEE Trans. Autom. Control*, vol. 40, no. 6, pp. 1083–1087, Jun. 1995.

[18] H. Habibi, H. R. Nohooji, and I. Howard, "Backstepping Nussbaum gain dynamic surface control for a class of input and state constrained systems with actuator faults," *Inf. Sci.*, vol. 482, pp. 27–46, May 2019.

[19] X.-S. Wang, C.-Y. Su, and H. Hong, "Robust adaptive control of a class of nonlinear systems with unknown dead-zone," *Automatica*, vol. 40, no. 3, pp. 407–413, Mar. 2004.

[20] S. Ibrir, W. F. Xie, and C.-Y. Su, "Adaptive tracking of nonlinear systems with non-symmetric dead-zone input," *Automatica*, vol. 43, no. 3, pp. 522–530, Mar. 2007.

[21] J.-H. Kim, J.-H. Park, S.-W. Lee, and E. K. P. Chong, "A two-layered fuzzy logic controller for systems with deadzones," *IEEE Trans. Ind. Electron.*, vol. 41, no. 2, pp. 155–162, Apr. 1994.

[22] R. R. Selmic and F. L. Lewis, "Deadzone compensation in motion control systems using neural networks," *IEEE Trans. Autom. Control*, vol. 45, no. 4, pp. 602–613, Apr. 2000.

[23] D. A. Recker, P. V. Kokotovic, D. Rhode, and J. Winkelman, "Adaptive nonlinear control of systems containing a deadzone," in *Proc. 30th IEEE Conf. Decis. Control*, Dec. 1991, pp. 2111–2115.

[24] J. Zhou and X. Z. Shen, "Robust adaptive control of nonlinear uncertain plants with unknown dead-zone," *IET Control Theory Appl.*, vol. 1, no. 1, pp. 25–32, Jan. 2007.

[25] Y. Jiang, Z. Liu, C. Chen, and Y. Zhang, "Adaptive robust fuzzy control for dual arm robot with unknown input deadzone nonlinearity," *Nonlinear Dyn.*, vol. 81, no. 3, pp. 1301–1314, Aug. 2015.

[26] X. Wang and S. Wang, "Adaptive fuzzy control with smooth inverse for nonlinear systems preceded by non-symmetric dead-zone," *Int. J. Syst. Sci.*, vol. 47, no. 9, pp. 2237–2246, Jul. 2016.

[27] B. Xu, "Robust adaptive neural control of flexible hypersonic flight vehicle with dead-zone input nonlinearity," *Nonlinear Dyn.*, vol. 80, no. 3, pp. 1509–1520, May 2015.

[28] Y. Wang and J. Hu, "Improved prescribed performance control for air-breathing hypersonic vehicles with unknown deadzone input nonlinearity," *ISA Trans.*, vol. 79, pp. 95–107, Aug. 2018.

[29] Z. Dong, Y. Li, M. Lv, and R. Zuo, "Adaptive accurate tracking control of HFVs in the presence of dead-zone and hysteresis input nonlinearities," *Chin. J. Aeronaut.*, vol. 34, no. 5, pp. 642–651, May 2021.

[30] B. Xu, X. Wang, F. Sun, and Z. Shi, "Intelligent control of flexible hypersonic flight dynamics with input dead zone using singular perturbation decomposition," *IEEE Trans. Neural Netw. Learn. Syst.*, vol. 34, no. 9, pp. 5926–5936, Dec. 2021.

[31] A. Fekih, "Fault-tolerant flight control design for effective and reliable aircraft systems," *J. Control Decis.*, vol. 1, no. 4, pp. 299–316, Oct. 2014.

[32] P. Lu, E.-J. van Kampen, C. de Visser, and Q. Chu, "Aircraft fault-tolerant trajectory control using incremental nonlinear dynamic inversion," *Control Eng. Pract.*, vol. 57, pp. 126–141, Dec. 2016.

[33] X. Yu, Y. Fu, and Y. Zhang, "Aircraft fault accommodation with consideration of actuator control authority and gyro availability," *IEEE Trans. Control Syst. Technol.*, vol. 26, no. 4, pp. 1285–1299, Jul. 2018.

[34] Y. Ren, P. Zhu, Z. Zhao, J. Yang, and T. Zou, "Adaptive fault-tolerant boundary control for a flexible string with unknown dead zone and actuator fault," *IEEE Trans. Cybern.*, vol. 52, no. 7, pp. 7084–7093, Jul. 2022.

[35] Z. Zhao, Z. Tan, Z. Liu, M. Ö. Efe, and C. K. Ahn, "Adaptive inverse compensation fault-tolerant control for a flexible manipulator with unknown dead-zone and actuator faults," *IEEE Trans. Ind. Electron.*, vol. 70, no. 12, pp. 12698–12707, Dec. 2023.

[36] H. Habibi, A. Yazdani, M. Darouach, H. Wang, T. Fernando, and I. Howard, "Observer-based sensor fault-tolerant control with prescribed tracking performance for a class of nonlinear systems," *IEEE Trans. Autom. Control*, vol. 68, no. 12, pp. 8259–8266, Dec. 2023.

[37] C. Wang and Y. Lin, "Decentralized adaptive tracking control for a class of interconnected nonlinear time-varying systems," *Automatica*, vol. 54, pp. 16–24, Apr. 2015.

[38] X. Wang, Z. Chen, and G. Yang, "Finite-Time-Convergent differentiator based on singular perturbation technique," *IEEE Trans. Autom. Control*, vol. 52, no. 9, pp. 1731–1737, Sep. 2007.

[39] G. H. Hardy, J. E. Littlewood, and G. Polya, *Inequalities*. Cambridge, U.K.: Cambridge Univ. Press, 1952.

YOUFANG YU received the B.S. degree in electronic engineering and the M.S. degree in agricultural electrification and automation from Zhejiang University, Hangzhou, in 1999 and 2006, respectively. From 1999 to 2003, she was a Lecturer with Anhui Vocational and Technical College, Hefei. From 2006 to 2008, she became an Electronic Engineer with the Research and Development Department, Zhejiang Jincheng Technology Development Company Ltd., Hangzhou. Since 2008, she has been with the Applied Engineering College, Zhejiang Business College, Hangzhou, where she is currently an Associate Professor. Her current research interests include automatic control, industrial automation, electronic technology, and biomass technology.

LIYANG WANG received the B.S. degree in telecommunication engineering from Xidian University, Xi'an, in 2019, and the M.S. degree in information and communication engineering from Southeast University, Nanjing, in 2022. Since 2023, he has been an Assistant with the Applied Engineering College, Zhejiang Business College, Hangzhou. His current research interests include B5G/6G mobile communication technology and electronic technology.